

Tunneling ionization in ultrashort laser pulses: Edge effect and remedyM. Klaiber ^{*}, Q. Z. Lv [†], K. Z. Hatsagortsyan , and C. H. Keitel 
Max-Planck-Institut für Kernphysik, Saupfercheckweg 1, 69117 Heidelberg, Germany (Received 19 January 2022; revised 5 May 2022; accepted 6 June 2022; published 22 June 2022)

Tunneling ionization of an atom in ultrashort laser pulses is considered. When the driving laser pulse is switched on and off with a steep slope, the photoelectron momentum distribution (PMD) shows an edge effect because of the photoelectron diffraction by the time slit of the pulse. The trivial diffraction pattern of the edge effect consisting of fast oscillations in the PMD disguises in the deep nonadiabatic regime the physically more interesting features in the spectrum, which originate from the photoelectron dynamics. We point out the precise conditions for how to avoid this scenario experimentally, and if unavoidable in theory we put forward an efficient method to remove the edge effect in the PMD. This allows us to highlight the nonadiabatic dynamical features of the PMD, which will be indispensable in additional investigations in complex computationally demanding scenarios. The method is first demonstrated with a one-dimensional problem, and further applied in three dimensions for the attoclock. The method is validated by a comparison of analytical results via the strong-field approximation with numerical solutions of the time-dependent Schrödinger equation.

DOI: [10.1103/PhysRevA.105.063109](https://doi.org/10.1103/PhysRevA.105.063109)**I. INTRODUCTION**

Modern state-of-the-art laser techniques allow for full control over the wave form of a laser pulse, and in particular the generation of few-cycle strong laser pulses [1–6] and even half-cycle pulses [7–10]. Few-cycle laser pulses of sufficient strength are an efficient tool in attoscience [11–13]. They have been employed for the generation of isolated attosecond pulses via high-order harmonic generation (HHG) [14–17], for molecular imaging and laser-induced electron diffraction [18–21], as well as for the time-resolved study of strong-field phenomena, such as nonsequential double ionization [22–29] and dissociative ionization [30,31]. The theoretical description of strong-field phenomena in few-cycle pulses within the strong field approximation (SFA) is outlined in Ref. [32].

In ultrashort laser pulses, an abrupt switch on and off of the laser pulse can induce a diffraction effect of the photoelectrons by the time slit of the pulse due to the pulse edges, the so-called edge effect. The edge effect is exhibited as oscillations in the photoelectron momentum distribution (PMD), in addition to the dynamical features of PMD, and it disappears in the case of a smooth laser pulse. The edge effect distorts the most important dynamical physical signal in strong-field ionization, and for this reason one tries to avoid or separate it. The distortion is especially conspicuous at low

laser intensities when the ionization signal is weak, but just in this deeply nonadiabatic regime the dynamical features of PMD are nontrivial. We underline that there are observed unexplained features in PMD in elliptically polarized laser fields in the weak-field regime [33,34], and the edge effect hinders their analysis.

In an experiment, the role of edge effects could be diminished using increasingly smooth laser pulses. In a theoretical description via numerical solution of the time-dependent Schrödinger equation (TDSE), as well as within the SFA, different forms of laser pulses with a smooth switch on and off are employed. The simplest description of a short N -cycle laser pulse is via a \cos^2 envelope: $f(t) = \cos^2(\omega t/N)$, with the laser frequency ω ; see, e.g., [32,35]. Smoother pulses are obtained via \cos^n envelopes with $n = 4$ or larger (in this case, one needs to take into account the change of the effective frequency of the laser field). A better description is obtained with the use of a Gaussian pulse with a long tail [36], which, however, requires rather time-consuming computationally expensive calculations. As the laser pulse shaping technique is presently well advanced, one cannot exclude the generation of the edge effect in experiments (e.g., using a laser pulse similar to a \cos^2 pulse), although up to now there has been no confirmed report on this point.

In this paper, we put forward a simple method to separate the edge effect and single out the PMD dynamical signal in SFA calculations as well as in the numerical solution of the TDSE, while using laser pulses with no-smooth switching. The (U-contour) method mimics the saddle-point integration, but without explicitly finding and classifying *all* relevant saddle points for the given PMD. We demonstrate the method in a one-dimensional (1D) model of tunneling ionization in half-cycle pulses of \cos^2 and truncated-Gaussian form, and we confirm its accuracy in comparison with the numerical TDSE solution. Finally, we apply the method in a 3D example of the

^{*}klaiber@mpi-hd.mpg.de[†]qingzheng.lyu@mpi-hd.mpg.de

Published by the American Physical Society under the terms of the Creative Commons Attribution 4.0 International license. Further distribution of this work must maintain attribution to the author(s) and the published article's title, journal citation, and DOI. Open access publication funded by the Max Planck Society.

attoclock. The U-contour method in 3D has a clear advantage with respect to the saddle-point integration, as the latter would require the calculation of a large data set of saddle points.

The structure of the paper is the following. In Sec. II the SFA model is introduced, and the edge effect is described. The conditions for the appearance of the effect are discussed in Sec. III. The U-contour method for separation of the edge effect is introduced in Sec. IV, and its performance is tested in comparison with numerical solutions of the TDSE. The application of the U-contour method for the analysis of the edge effect in the 3D case of an attoclock is presented in Sec. V, and the conclusion is given in Sec. VI.

II. EDGE EFFECT AND THEORETICAL DESCRIPTION

We consider ionization of an electron bound in an atomic potential $V(r)$ in a laser pulse with electric field $\mathbf{E}(t)$. The asymptotic momentum distribution,

$$w(p) = |m(p)|^2, \quad (1)$$

is determined by the SFA direct ionization amplitude [37]:

$$m(p) = -i \int dt \langle \psi_p^V(t) | H_i(t) | \phi(t) \rangle, \quad (2)$$

where $\phi(\mathbf{r}, t)$ is the bound state wave function, $\psi_p^V(\mathbf{r}, t)$ the Volkov wave function [38], and $H_i(t) = \mathbf{r} \cdot \mathbf{E}(t)$ is the electron interaction Hamiltonian with the laser field. Atomic units are used throughout. The integrals in the amplitudes of Eqs. (2) are calculated in two ways: fully numerically and with the saddle-point approximation (SPA) analytically.

We illustrate the edge effect on a 1D problem of ionization of an electron bound in a 1D zero-range potential $V(x) = -\kappa\delta(x)$, in a half-cycle laser pulse with electric field $E(t) = -E_0 \cos^2(\omega t)$ along the x -coordinate, with the field vanishing at $t < t_i$ and $t > t_f$. The unipolar feature of the pulse is not significant for the edge effect, but it is significant how fast the pulse is switched on/off. The half-cycle pulse is used to avoid recollisions and intercycle interferences, which will produce some features in the spectrum, masking the discussed edge effect. Here $\omega = 0.05$ a.u., $\kappa = \sqrt{2}I_p = 1$ a.u., I_p is the ionization potential, and $\gamma = \tilde{\omega}\kappa/E_0$ is the Keldysh parameter, with the effective frequency $\tilde{\omega} \equiv \sqrt{2}\omega$ related to the \cos^2 pulse [the effective frequency is defined as $\tilde{\omega} = \sqrt{-E''(0)/E(0)}$ at the field maximum $t = 0$]. We calculate PMD for different laser fields, using the SFA amplitude of Eq. (2), with the bound state wave function $\phi(x, t) = \sqrt{\kappa} \exp(-\kappa|x| + i\kappa^2/2t)$. The results are presented in Figs. 1–3.

In strong fields, the PMD is a smooth function of the asymptotic momentum; see the case of $E_0 = 0.1$ a.u. for the \cos^2 pulse in Fig. 1(a), and for truncated Gaussian pulses in Figs. 2(a) and 2(c). In contrast, at weak fields PMD appears to be superimposed by the diffraction pattern due to the time slit of the pulse edges; see $E_0 = 0.05$ and 0.025 a.u. in Figs. 1(b) and 1(c) for the \cos^2 pulse, and Figs. 2(b) and 2(d) for Gaussian pulses, respectively (orange-dashed lines in the figures correspond to the SFA, and green-dotted lines to the TDSE numerical solutions). This effect is large in weak fields, when the ionization dynamical signal is weak, and strongly dependent on the pulse shape. In fact, in a

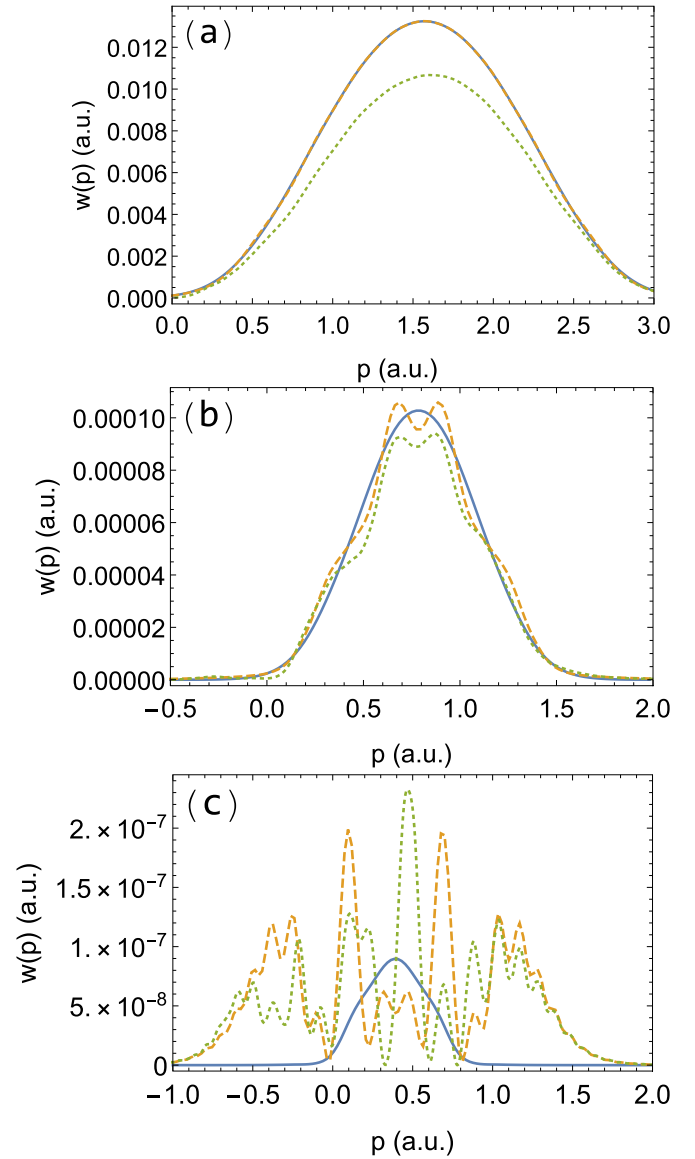


FIG. 1. PMD with a field $E(t) = -E_0 \cos^2(\omega t)$. (a) $E_0 = 0.1$, (b) $E_0 = 0.05$, (c) $E_0 = 0.025$. $\omega = 0.05$ a.u., $\kappa = 1$ a.u., and the field is truncated at $\omega t_i = -\pi/2$ and $\omega t_f = \pi/2$. The orange dashed line: via the SFA with the edge-effect; the blue solid line: via the SFA with the edge effect subtracted; the dotted green line: via numerical solution of the TDSE.

Gaussian pulse $E(t) = -E_0 \exp[-(\omega t)^2]$ of the same effective frequency ($\omega = 0.05$) as a \cos^2 pulse, the edge effect gradually decreases with increasing Gaussian truncation. In particular, the edge effect vanishes, i.e., oscillations in PMD disappear, if a rather large truncation time is applied; see the green-dotted lines in Figs. 2(b), 2(d) and 3 corresponding to $\omega(t_f - t_i) = 16$. However, the edge effect persists at smaller truncation time at the same field strength and the same frequency; see the dashed lines in Figs. 2(b) and 2(d) corresponding to $\omega(t_f - t_i) = 4$. While the use of Patchkovskii's smoothly truncated Gaussian pulse of Ref. [36] decreases the edge effect (see the red-dot-dashed line in Fig. 3), at weak fields the boundary terms still contribute and contaminate the physical PMD.

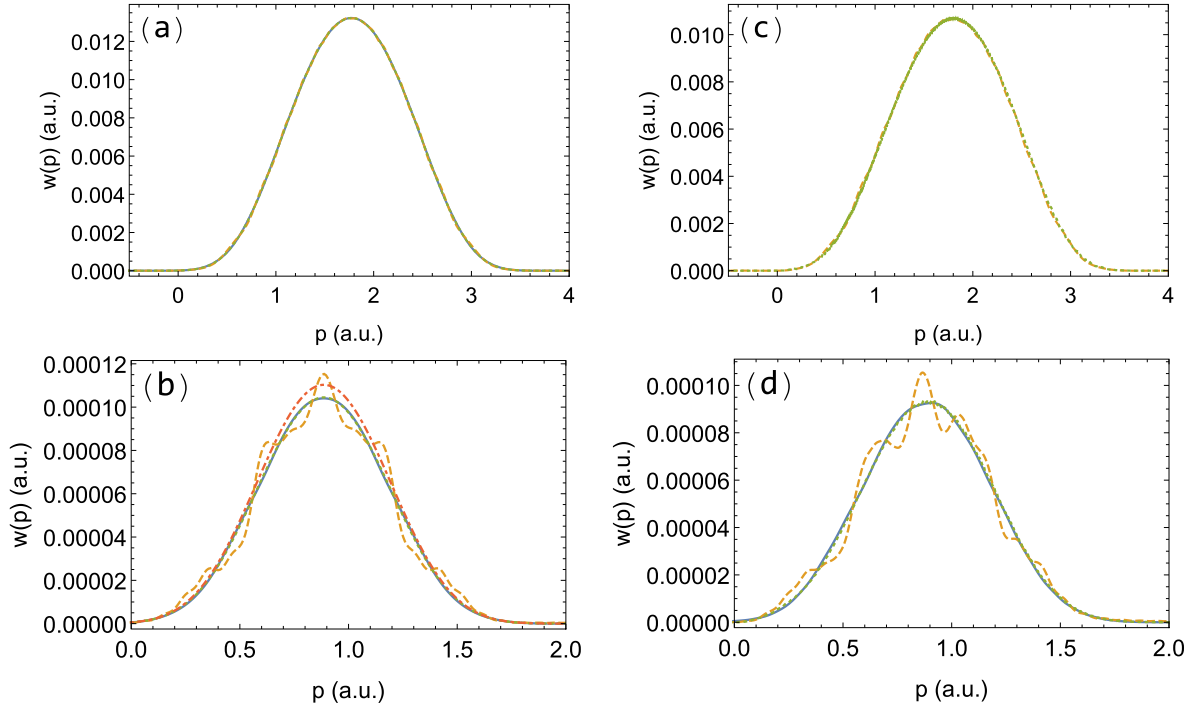


FIG. 2. PMD with a field $E(t) = -E_0 \exp[-(\omega t)^2]$. Left column: via the first-order SFA, Eq. (1); right column: via numerical solution of the TDSE. (a), (c) $E_0 = 0.1$; (b), (d) $E_0 = 0.05$. The dashed orange line denotes short pulses with the truncation points of the Gaussian at $\omega t_i = -2$ and $\omega t_f = 2$; the dotted green line denotes long pulses with $\omega t_i = -8$ and $\omega t_f = 8$; the blue solid line denotes the edge effect subtracted; the red dot-dashed line in (b) is the SFA calculation with SPA. $\omega = 0.05$ a.u., $\kappa = 1$ a.u.

In Figs. 1–3, we provide PMD via the SFA, as well as via the numerical solution of the TDSE. For strong fields $E_0 = 0.1$ and 0.05 , the SFA results are in close agreement with the numerical ones in any pulse. Deviations mainly originate from the Stark shift, which is not accounted for in the SFA, yielding slightly overestimated ionization probabilities. In weak fields, $E_0 = 0.025$, the results are still in agreement with long Gaussian pulses, but in short truncated-Gaussian pulses the edge effects are different in the SFA and in the TDSE, concurring only qualitatively.

III. CONDITIONS FOR THE EDGE-EFFECT APPEARANCE

Generally, the smoother the switching on and off of the laser pulse is, the less pronounced are the edge effects. However, for a given smooth pulse shape, there is a threshold intensity below which the edge effects again show up. This is illustrated for \cos^n -type pulses in Fig. 4. We estimate the condition for the edge-effect appearance as follows. The switching on/off of the laser pulse results in the appearance of high-energy components in the field spectrum. The edge

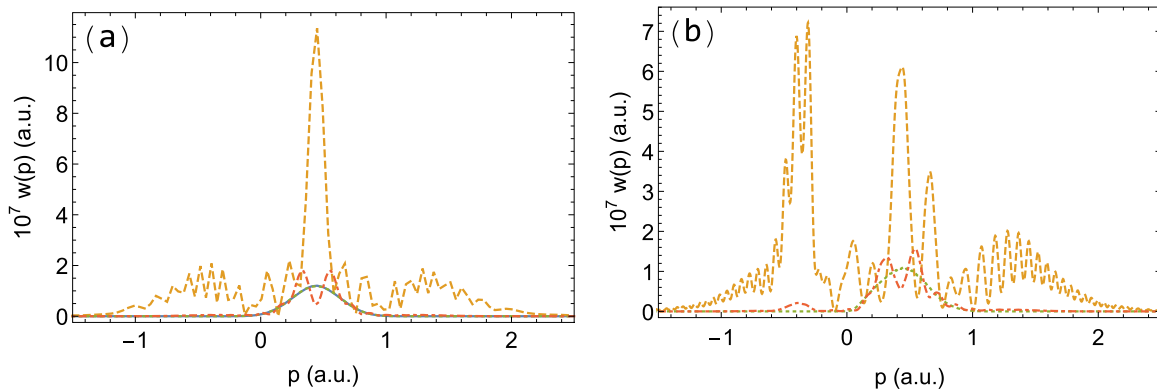


FIG. 3. PMD with a field $E(t) = -E_0 \exp[-(\omega t)^2]$, $E_0 = 0.025$. (a) Via the first-order SFA, (b) via numerical solution of the TDSE. The dashed orange line denotes short pulses with the truncation points of the Gaussian at $\omega t_i = -2$ and $\omega t_f = 2$; the dotted green line denotes long pulses with $\omega t_i = -8$ and $\omega t_f = 8$; the blue solid line denotes the SFA with the edge effect subtracted; the dot-dashed red line is via Patchkowsii's truncated Gaussian [36] with parameters $\omega t_1 = 2$ and $\omega t_2 = 2.5$. $\omega = 0.05$ a.u., $\kappa = 1$ a.u.

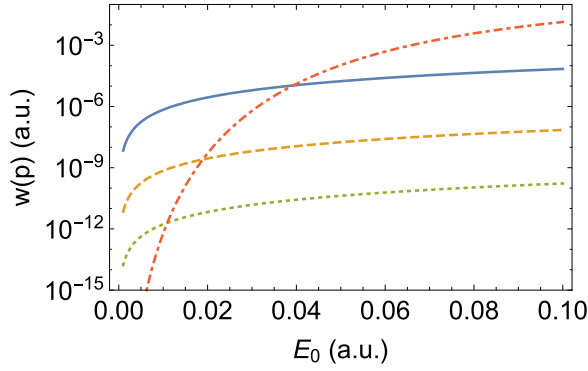


FIG. 4. Determination of the threshold field strength in \cos^n pulses, below which the edge effect contaminates the strong-field ionization PMD. The edge effect is induced by the high-energy component of the field with $\Omega \gtrsim I_p$, the probability of photoionization W_Ω via such high-energy photon absorption: The blue solid line, \cos^2 pulse; the orange dashed line, \cos^4 pulse; the green short-dashed line, \cos^6 pulse; the red dash-dotted line, the PPT probability W_{SFI} . The edge effect will be visible below the field value when $W_\Omega = W_{\text{SFI}}$.

effect is induced by the high-energy component of the field with $\Omega \gtrsim I_p$, available in the spectrum of the pulse. We characterize the edge effect by the probability of photoionization via absorption of such a high-energy photon [39]:

$$W_\Omega \sim \left(\frac{E_\Omega a}{\Omega} \right)^2, \quad (3)$$

with the field strength $E_\Omega \sim E_0(\omega/\Omega)^n$ of the high-frequency component Ω , and the typical atomic length $a = 1/\kappa$. The edge effect will be visible if this probability is comparable with (or larger than) the strong-field ionization probability [40] due to the monochromatic field of the effective frequency of the pulse:

$$W_{\text{SFI}} \sim \frac{E_a}{E_s} \exp \left\{ -\frac{2I_p}{\tilde{\omega}} \left[\left(1 + \frac{1}{2\gamma^2} \right) \text{arcsinh} \gamma - \frac{\sqrt{1 + \gamma^2}}{2\gamma} \right] \right\}, \quad (4)$$

where $E_s = E_0 \sqrt{1 + \gamma^2}$ is the field value at the time saddle point. Thus, the condition of the onset of the edge effect is $W_\Omega \gtrsim W_{\text{SFI}}$. In Fig. 4, $W_\Omega = W_{\text{SFI}}$ corresponds to the crossing point of the red line representing W_{SFI} with the corresponding one-photon probabilities W_Ω for different pulses. Thus, the edge effect will be visible in the corresponding pulses with the field strength below the crossing points. The smoother the laser pulse is, the smaller will be the laser intensity below which the edge effect will emerge. The edge effect appears at low laser intensities, when the tunneling ionization signal is weak and becomes comparable with the diffraction signal. This effect hinders the understanding of nonadiabatic tunneling at large Keldysh parameters, as it conceals specific nonadiabatic features in PMD.

IV. SEPARATION OF THE EDGE EFFECT

In this section, we put forward a method for separation of the edge effect and singling out the dynamical features of PMD at given laser parameters. In the total PMD with the edge effect, the dynamical signal is superimposed by the trivial diffraction pattern due to the time slit of the pulse. Meanwhile,

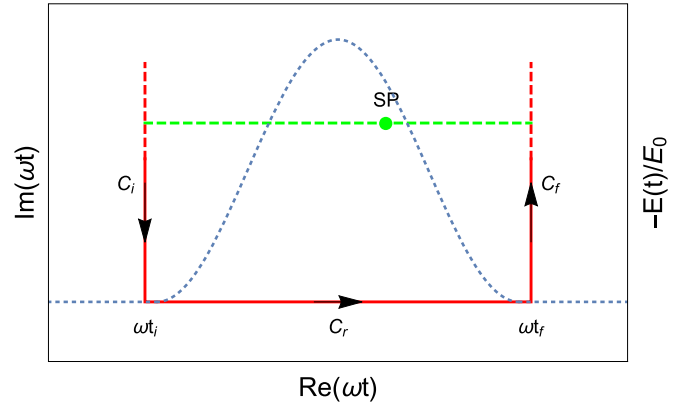


FIG. 5. Contours of the time integration in Eqs. (5) and (17): red horizontal line, the original contour along the real-time axis from the pulse outset t_i to the end t_f ; green dashed line, the saddle-point (SP) contour; red solid line, the proposed U-contour to remove the pulse edge effect. The laser pulse form is illustrated via the blue dashed line.

the dynamical signal is most interesting physically because it provides information on the nonadiabatic dynamics of the photoelectron in a weak-field regime. As an example, we refer to structures inside the attoclock ring in a weak elliptically polarized laser field [34], which also could be related to the unexplained large attoclock offset angles in the multiphoton regime [33].

A. U-contour method

Before introducing the method for separation of the edge effects, let us note that the edge effect can be avoided in the calculation of PMD within the SFA, when using the SPA for the time integration; see, e.g., the red-dashed line in Fig. 2(b) [41]. However, in 3D cases and for a large range of PMD, e.g., in the attoclock (see Sec. V), it is a cumbersome procedure to find all saddle points of the full PMD. Moreover, there still remains the question of how to remove the edge effect for the TDSE. In the latter, the only possibility is to use a Gaussian pulse with a very large truncation time, which requires extensive computational resources.

Here we propose a simple method for the calculation of the edge-effect-free PMD. The method mimics the saddle-point time-integration method for the ionization amplitude. In the first-order SFA, the integrand $m(t)$ of the ionization amplitude,

$$m(p) = \int_{t_i}^{t_f} dt m(t), \quad (5)$$

has the form

$$m(t) = C \frac{[\mathbf{p} + \mathbf{A}(t)] \cdot \mathbf{E}(t)}{[|\mathbf{p} + \mathbf{A}(t)|^2 + \kappa^2]^2} \exp[-iS(t) + i\kappa^2/2t], \quad (6)$$

with the classical action in the laser field $S(t) = \int_{t_i}^t ds [\mathbf{p} + \mathbf{A}(s)]^2/2$, and the constant $C_{1D} = -2i\sqrt{\frac{2}{\pi}}\kappa^{3/2}$ for the 1D case, and $C_{3D} = 1/(\sqrt{2\pi}\kappa)C_{1D}$ for the 3D case. In the original Eq. (5), the time integration runs along the real-time axis from the onset of the pulse t_i to the end t_f ; see Fig. 5.

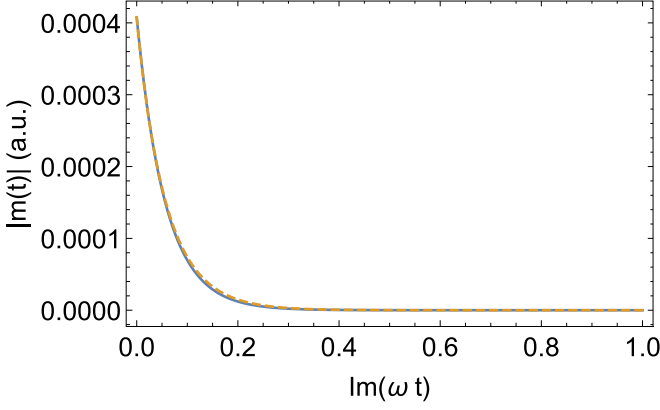


FIG. 6. The amplitude of the integrand along the vertical contour, exactly (blue solid line) and approximated by the expansion of Eq. (7) (orange dashed line).

When one applies the SPA, the original contour is deformed to the steepest-descent contour of the saddle point. Generally, one has to find all saddle points corresponding to the given asymptotic momentum via an appropriate deformation of the initial contour of the time integration. As is shown in Fig. 5, the integral along the steepest-descent contour is equal to that along the U-contour (red line in Fig. 5). Thus, the edge-free PMD can be obtained adding two integrals along the vertical contour to the main integral along the real axis (from t_i to t_f). This can be done analytically within the SFA, as well as numerically in the TDSE solution.

Further, we note that the U-contour can also be used to calculate half-cycle resolved ionization probabilities in long sinusoidal fields via truncating the field at the beginning and the end of the half-cycle of interest.

B. Calculation of the time integral along the vertical contour

The calculation of the time integrals along the vertical contours in Fig. 5, C_i and C_f , is facilitated by the fact that the integrand is exponentially suppressed at large imaginary times, see Fig. 6, and only the beginning of the contour close to the real axis gives the main contribution to the integral. This is the case when the complex continuation of the functional form of the laser pulse is analytical within the U-contour. This is particularly valid for the \cos^n pulses and a truncated Gaussian.

To account for the edge effect analytically, we approximate the prefactor and the exponential of the integrand $m(t)$ near the truncation points t_i and t_f :

$$m_{C_i}(t) \approx C \sum_n \frac{[p + A(t_i)]A^{n+1}(t_i)(t - t_i)^n}{n!([p + A(t_i)]^2 + \kappa^2)^2} \times \exp[-iS(t_i) + i\kappa^2/2t_i + i\{\kappa^2/2 + [p + A(t_i)]^2/2\}(t - t_i)], \quad (7)$$

$$m_{C_f}(t) \approx C \sum_n \frac{[p + A(t_f)]A^{n+1}(t_f)(t - t_f)^n}{n!([p + A(t_f)]^2 + \kappa^2)^2} \times \exp[-iS(t_f) + i\kappa^2/2t_f + i\{\kappa^2/2 + [p + A(t_f)]^2/2\}(t - t_f)], \quad (8)$$

where the summation over n begins from the first nonvanishing derivative of the function $A'(t)$ up to the next high orders at weak fields, and terms of the order of $A'(t_i)^2$ or $A'(t_f)^2$ are neglected. These approximated integrands can now be integrated along the steepest-descent contour at the truncation points. Since $\kappa^2/2 + [p + A(t_i)]^2/2$ and $\kappa^2/2 + [p + A(t_f)]^2/2$ are real numbers, the contour is vertically aligned in the complex plane starting at t_i or t_f , respectively. The integration yields

$$m_{C_i}(p) = C \sum_n 2^{n+1} \exp[-iS(t_i) + i\kappa^2/2t_i] \times \frac{[p + A(t_i)]A^{n+1}(t_i)}{\{[p + A(t_i)] + \kappa^2\}^{n+3}}, \quad (9)$$

$$m_{C_f}(p) = C \sum_n 2^{n+1} \exp[-iS(t_f) + i\kappa^2/2t_f] \times \frac{[p + A(t_f)]A^{n+1}(t_f)}{\{[p + A(t_f)] + \kappa^2\}^{n+3}}. \quad (10)$$

The approximated integrand function of Eq. (9) is shown in Fig. 6. It coincides with the analytical one. Thus, using expressions of Eqs. (9) and (10), the contribution of the vertical contours C_i , C_f can be subtracted analytically, which corresponds to the subtraction of the edge effect.

C. Edge-effect subtraction in the numerical solution of the TDSE

The PMD according to numerical solution of the TDSE can be written as

$$w(p) = |m(p)|^2 = |\langle \psi_p^V(x, t_f) | U(t_f, t_i) | \phi(x, t_i) \rangle|^2, \quad (11)$$

where the time evolution operator $U(t_f, t_i)$ can be obtained through the normal Schrödinger equation

$$U(t_f, t_i) = \mathcal{T} \exp \left[-i \int_{t_i}^{t_f} dt H(t) \right], \quad (12)$$

with $H(t) = \hat{\mathbf{p}}^2/2m + \mathbf{r} \cdot \mathbf{E}(t) + V(\mathbf{r})$, and \mathcal{T} being the time ordering operator, or based on the Dyson equation

$$U(t_f, t_i) = U_0(t_f, t_i) - i \int_{t_i}^{t_f} dt U(t_f, t) H_i(t) U_0(t, t_i), \quad (13)$$

with $H_i(t) = \mathbf{r} \cdot \mathbf{E}(t)$ being the interaction Hamiltonian, and U_0 being the field-free time evolution operator.

The ionization amplitude $m(p)$ along the real axis is calculated as

$$m_{C_r}(p) = \langle \psi_p^V(t_f) | \mathcal{T} \exp \left[-i \int_{t_i}^{t_f} dt H(t) \right] | \phi(t_i) \rangle \quad (14)$$

employing the traditional time-splitting operator method. Along the vertical contours (C_i and C_f), on the other hand, the amplitude is obtained through

$$m_{C_i}(p) = -i \int_{C_i} dt \langle \psi_p^V(t_f) | U(t_f, t) H_i(t) U_0(t, t_i) | \phi(t_i) \rangle, \quad (15)$$

$$m_{C_f}(p) = -i \int_{C_f} dt \langle \psi_p^V(t_f) | U(t_f, t) H_i(t) U_0(t, t_i) | \phi(t_i) \rangle. \quad (16)$$

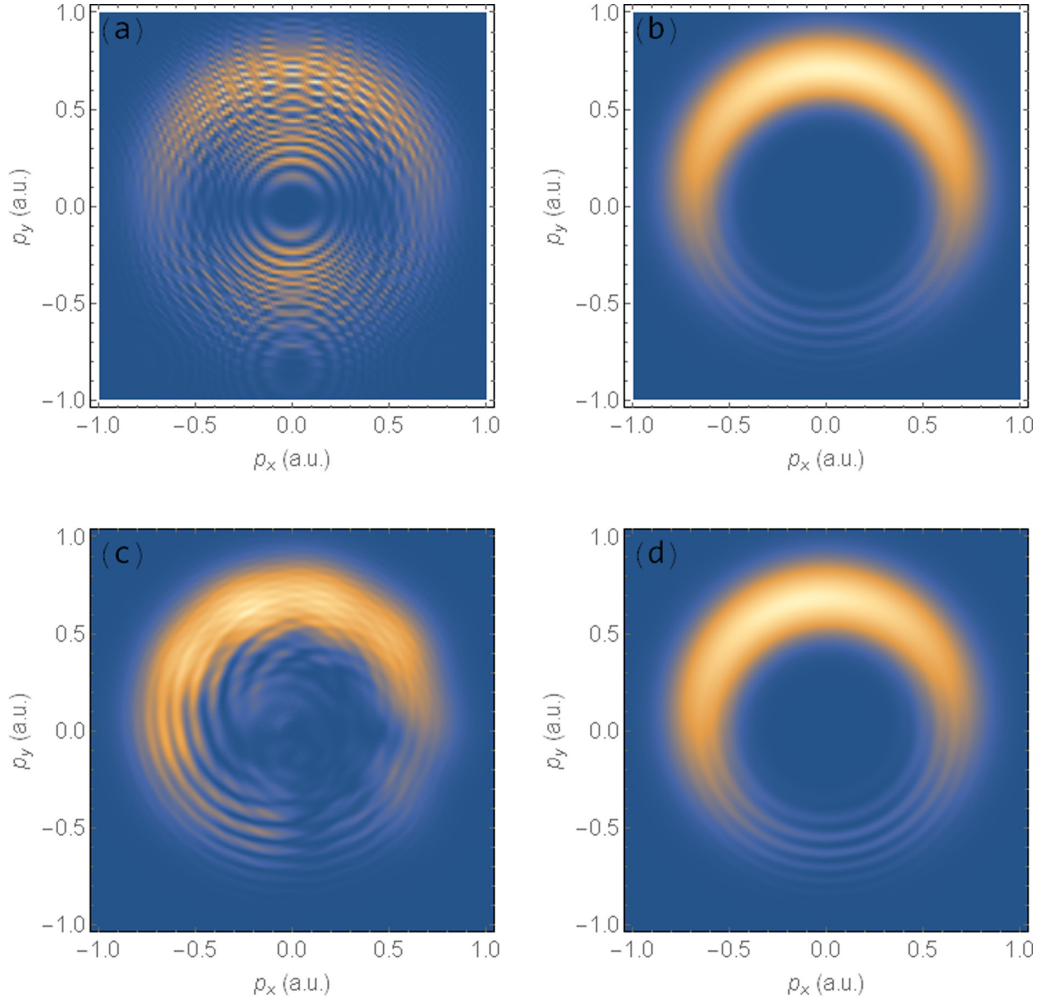


FIG. 7. PMD in the attoclock: (a), (b) via the first-order SFA; (c), (d) via numerical solution of the TDSE; (a), (c) PMD with the edge effect included, (b), (d) PMD with the edge effect subtracted. The laser field in (a)–(c) is given by Eq. (18), while in (d) it is given by Eq. (19). $E_0 = 0.025$ a.u., $\omega = 0.05$ a.u., $\kappa = 1$ a.u., and the field truncation is at $\omega t_i = -3\pi/\omega$ and $\omega t_f = 3\pi/\omega$.

Here $U(t_f, t)$ is the exact time-evolution operator in the numerical simulation rather than the time-evolution operator in the laser pulse only, which is used in the SFA calculations.

Finally, the total PMD is calculated as

$$w(p) = |m_{C_r}(p) + m_{C_i}(p) + m_{C_f}(p)|^2. \quad (17)$$

V. ATTOCLOCK

The proposed U-contour method proves very efficient for the calculation of PMD of the attoclock at weak laser intensities. We calculate PMD via the 3D first-order SFA in the attoclock case for a hydrogen atom with a circularly polarized laser field given by the vector potential

$$\begin{aligned} A_x(t) &= \frac{E_0}{\omega} \sin(\omega t) \cos^2(\omega t/6), \\ A_y(t) &= -\frac{E_0}{\omega} \cos(\omega t) \cos^2(\omega t/6), \end{aligned} \quad (18)$$

with $E_0 = 0.025$ a.u., $\omega = 0.05$ a.u., $\kappa = 1$ a.u., a Coulomb atomic potential, and the laser field truncation at $\omega t_i = -3\pi/\omega$ and $\omega t_f = 3\pi/\omega$. The time integral in Eq. (5) is

calculated numerically, and the edge terms are subtracted analytically as shown above. The corresponding momentum distributions via the SFA are presented in Figs. 7(a) and 7(b). We compare the latter with the numerical TDSE calculations; see Figs. 7(c) and 7(d). To eliminate the edge effect in the numerical TDSE case, we employ a smooth pulse of the form

$$\begin{aligned} A_x(t) &= \frac{E_0}{\omega} \sin(\omega t) \cos^8(\omega t/12), \\ A_y(t) &= -\frac{E_0}{\omega} \cos(\omega t) \cos^8(\omega t/12). \end{aligned} \quad (19)$$

Note that in a long Gaussian pulse, the PMD coincides with the edge-effect-free result of the U-contour method. One can see that the edge effects significantly disturb PMD. In particular, the edge effect is seen in Fig. 7(a) as a diffraction pattern on the time slit of the pulse, which is superimposed over the attoclock typical distribution [Fig. 7(b)]. The diffraction pattern is also distinguishable in the TDSE calculations [Fig. 7(c)], which disappears in a smooth laser pulse [Fig. 7(d)]. The U-contour method efficiently removes the edge effect [Fig. 7(b)], and its result is similar to that in a

smooth laser pulse. Note that the PMD in the TDSE calculations shows a non-negligible offset angle due to the Coulomb field of the atomic core. The latter is not accounted for in the first-order SFA calculation, which, consequently, exhibits no offset angle.

The edge effect is usually prominent in weak laser fields, where it dominates over the weak ionization signal. In the example of Fig. 7, the total ionization probability is of the order of 5×10^{-6} , which is still observable being comparable with the ionization yield at weak fields in the experiment [42].

The edge effect is produced by the time slit of the laser pulse. When the laser pulse is described via the vector potential, the pattern of the edge effect in PMD follows the vector potential, similar to that due to tunneling ionization. However, if the laser pulse is described via the field, the pattern of the edge effect will follow the field structure, and the created PMD pattern of the edge effect in a circularly polarized laser field will be rotated with respect to that of tunneling ionization by the $\pi/2$ angle.

VI. CONCLUSION

We have developed a method to remove the edge effect of the laser pulse because of the diffraction from the time slit created by the edges in PMD of tunnel-ionized electrons. The method consists of replacing the original time integral in the ionization amplitude along the real-time axis with the so-called U-contour, adding two integrals along the imaginary-time axis, starting at the time edges of the laser pulse. The method can be applied analytically for the SFA as well as for the numerical solution of the TDSE. The edge effect adds a trivial diffraction pattern that originated from the time edges of the laser pulse, which disappear when using smoother laser pulses (long-truncated-Gaussian pulse) of the same frequency and intensity. The edge effect hides the physical structures in PMD due to nonadiabatic processes in weak laser fields that underline the important application of the proposed method to reveal the dynamical signal of strong-field ionization in the deep nonadiabatic regime.

-
- [1] T. Brabec and F. Krausz, Intense few-cycle laser fields: Frontiers of nonlinear optics, *Rev. Mod. Phys.* **72**, 545 (2000).
- [2] G. G. Paulus, F. Lindner, H. Walther, A. Baltuška, E. Goulielmakis, M. Lezius, and F. Krausz, Measurement of the Phase of Few-Cycle Laser Pulses, *Phys. Rev. Lett.* **91**, 253004 (2003).
- [3] E. Goulielmakis, M. Uiberacker, R. Kienberger, A. Baltuska, V. Yakovlev, A. Scrinzi, T. Westerwalbesloh, U. Kleineberg, U. Heinzmann, M. Drescher, and F. Krausz, Direct measurement of light waves, *Science* **305**, 1267 (2004).
- [4] S. Hrisafov, J. Pupeikis, P.-A. Chevreuril, F. Brunner, C. R. Phillips, L. Gallmann, and U. Keller, High-power few-cycle near-infrared opcpa for soft x-ray generation at 100 khz, *Opt. Express* **28**, 40145 (2020).
- [5] R. Piccoli, J. M. Brown, A. Jeong, Y.-G. Rovere, L. Zanotto, M. B. Gaarde, F. Légaré, A. Couairon, J. C. Travers, R. Morandotti, B. E. Schmidt, and L. Razzari, Intense few-cycle visible pulses directly generated via nonlinear fibre mode mixing, *Nat. Photon.* **15**, 884 (2021).
- [6] A. M. Zheltikov, Supercontinuum generation by ultrashort laser pulses, *Phys. Usp.* **49**, 605 (2006).
- [7] M. T. Hassan, T. T. Luu, A. Moulet, O. Raskazovskaya, P. Zhokhov, M. Garg, N. Karpowicz, A. M. Zheltikov, V. Pervak, F. Krausz, and E. Goulielmakis, Optical attosecond pulses and tracking the nonlinear response of bound electrons, *Nature (London)* **530**, 66 (2016).
- [8] Y. Shou, R. Hu, Z. Gong, J. Yu, J. erh Chen, G. Mourou, X. Yan, and W. Ma, Cascaded generation of isolated sub-10 attosecond half-cycle pulses, *New J. Phys.* **23**, 053003 (2021).
- [9] A. V. Bogatskaya, E. A. Volkova, and A. M. Popov, Unipolar terahertz pulse formation in a nonequilibrium plasma channel formed by an ultrashort uv laser pulse, *Phys. Rev. E* **104**, 025202 (2021).
- [10] E. Siminos, I. Thiele, and C. Olofsson, Laser Wakefield Driven Generation of Isolated Carrier-Envelope-Phase Tunable Intense Subcycle Pulses, *Phys. Rev. Lett.* **126**, 044801 (2021).
- [11] P. B. Corkum and F. Krausz, Attosecond science, *Nat. Phys.* **3**, 381 (2007).
- [12] M. Y. Ivanov, R. Kienberger, A. Scrinzi, and D. M. Villeneuve, Attosecond physics, *J. Phys. B* **39**, R1 (2006).
- [13] F. Krausz and M. Ivanov, Attosecond physics, *Rev. Mod. Phys.* **81**, 163 (2009).
- [14] M. Drescher, M. Hentschel, R. Kienberger, G. Tempea, C. Spielmann, G. A. Reider, P. B. Corkum, and F. Krausz, X-ray pulses approaching the attosecond frontier, *Science* **291**, 1923 (2001).
- [15] P. Agostini and L. F. DiMauro, The physics of attosecond light pulses, *Rep. Prog. Phys.* **67**, 813 (2004).
- [16] F. Calegari, G. Sansone, S. Stagira, C. Vozzi, and M. Nisoli, Advances in attosecond science, *J. Phys. B* **49**, 062001 (2016).
- [17] T. Popmintchev, M. C. Chen, D. Popmintchev, P. Arpin, S. Brown, S. Alisauskas, G. Andriukaitis, T. Balciunas, O. D. Mucke, A. Pugzlys, A. Baltuska, B. Shim, S. E. Schrauth, A. Gaeta, C. Hernández-García, L. Plaja, A. Becker, A. Jaron-Becker, M. M. Murnane, and H. C. Kapteyn, Bright coherent ultrahigh harmonics in the keV x-ray regime from mid-infrared femtosecond lasers, *Science* **336**, 1287 (2012).
- [18] H. Niikura, F. Legare, R. Hasbani, M. Y. Ivanov, D. M. Villeneuve, and P. B. Corkum, Probing molecular dynamics with attosecond resolution using correlated wave packet pairs, *Nature (London)* **421**, 826829 (2003).
- [19] J. Itatani, J. Levesque, D. Zeidler, H. Niikura, H. Pépin, J. C. Kieffer, P. B. Corkum, and D. M. Villeneuve, Tomographic imaging of molecular orbitals, *Nature (London)* **432**, 867 (2004).
- [20] C. I. Blaga, J. Xu, A. D. DiChiara, E. Sistrunk, K. Zhang, P. Agostini, T. A. Miller, L. F. DiMauro, and C. D. Lin, Imaging ultrafast molecular dynamics with laser-induced electron diffraction, *Nature (London)* **483**, 194 (2012).
- [21] B. Wolter, M. G. Pullen, A.-T. T. Le, M. Baudisch, K. Doblhoff-Dier, A. Senftleben, M. Hemmer, C. D. Schröter, J. Ullrich, T. Pfeifer, R. Moshhammer, S. Gräfe, O. Vendrell, C. D. Lin, and

- J. Biegert, Ultrafast electron diffraction imaging of bond breaking in di-ionized acetylene, *Science* **354**, 308 (2016).
- [22] R. Moshhammer, B. Feuerstein, W. Schmitt, A. Dorn, C. D. Schröter, J. Ullrich, H. Rottke, C. Trupp, M. Wittmann, G. Korn, K. Hoffmann, and W. Sandner, Momentum Distributions of ne^{n+} Ions Created by an Intense Ultrashort Laser Pulse, *Phys. Rev. Lett.* **84**, 447 (2000).
- [23] V. R. Bhardwaj, S. A. Aseyev, M. Mehendale, G. L. Yudin, D. M. Villeneuve, D. M. Rayner, M. Y. Ivanov, and P. B. Corkum, Few Cycle Dynamics of Multiphoton Double Ionization, *Phys. Rev. Lett.* **86**, 3522 (2001).
- [24] A. Rudenko, K. Zrost, C. D. Schröter, V. L. B. de Jesus, B. Feuerstein, R. Moshhammer, and J. Ullrich, Resonant structures in the low-energy electron continuum for single ionization of atoms in the tunnelling regime, *J. Phys. B* **37**, L407 (2004).
- [25] X. Wang and J. H. Eberly, Effects of Elliptical Polarization on Strong-Field Short-Pulse Double Ionization, *Phys. Rev. Lett.* **103**, 103007 (2009).
- [26] M. Kübel, C. Burger, N. G. Kling, T. Pischke, L. Beaufore, I. Ben-Itzhak, G. G. Paulus, J. Ullrich, T. Pfeifer, R. Moshhammer, M. F. Kling, and B. Bergues, Complete characterization of single-cycle double ionization of argon from the nonsequential to the sequential ionization regime, *Phys. Rev. A* **93**, 053422 (2016).
- [27] A. Chen, M. Kübel, B. Bergues, M. F. Kling, and A. Emmanouilidou, Non-sequential double ionization with near-single cycle laser pulses, *Sci. Rep.* **7**, 7488 (2017).
- [28] Z. Chen, L. Zhang, Y. Wang, O. Zatsarinny, K. Bartschat, T. Morishita, and C. D. Lin, Pulse-duration dependence of the double-to-single ionization ratio of ne by intense 780-nm and 800-nm laser fields: Comparison of simulations with experiments, *Phys. Rev. A* **99**, 043408 (2019).
- [29] F. Liu, Z. Chen, T. Morishita, K. Bartschat, B. Böning, and S. Fritzsche, Single-cycle versus multicycle nonsequential double ionization of argon, *Phys. Rev. A* **104**, 013105 (2021).
- [30] M. F. Kling, C. Siedschlag, A. J. Verhoef, J. I. Khan, M. Schultze, T. Uphues, Y. Ni, M. Uiberacker, M. Drescher, F. Krausz, and M. J. Vrakking, Control of electron localization in molecular dissociation, *Science* **312**, 246 (2006).
- [31] H. Xu, Z. Li, F. He, X. Wang, A. Atia-Tul-Noor, D. Kiełpinski, R. T. Sang, and I. V. Litvinyuk, Observing electron localization in a dissociating H_2^+ molecule in real time, *Nat. Commun.* **8**, 15849 (2017).
- [32] D. B. Milošević, G. G. Paulus, D. Bauer, and W. Becker, Above-threshold ionization by few-cycle pulses, *J. Phys. B* **39**, R203 (2006).
- [33] A. S. Landsman, M. Weger, J. Maurer, R. Boge, A. Ludwig, S. Heuser, C. Cirelli, L. Gallmann, and U. Keller, Ultrafast resolution of tunneling delay time, *Optica* **1**, 343 (2014).
- [34] I. A. Ivanov and A. S. Kheifets, Strong-field ionization of he by elliptically polarized light in attoclock configuration, *Phys. Rev. A* **89**, 021402(R) (2014).
- [35] C. P. J. Martiny and L. B. Madsen, Ellipticity dependence of the validity of the saddle-point method in strong-field ionization by few-cycle laser pulses, *Phys. Rev. A* **78**, 043404 (2008).
- [36] S. Patchkovskii and H. Müller, Simple, accurate, and efficient implementation of 1-electron atomic time-dependent Schrödinger equation in spherical coordinates, *Comput. Phys. Commun.* **199**, 153 (2016).
- [37] W. Becker, F. Grasbon, R. Kopold, D. B. Milošević, G. G. Paulus, and H. Walther, Above-threshold ionization: From classical features to quantum effects, *Adv. At. Mol. Opt. Phys.* **48**, 35 (2002).
- [38] D. M. Wolkow, Über eine Klasse von Lösungen der Diracschen Gleichung, *Z. Phys.* **94**, 250 (1935).
- [39] N. B. Delone and V. P. Krainov, *Multiphoton Processes in Atoms*, Springer Series on Atoms+Plasmas (Springer, Berlin, 2000).
- [40] V. S. Popov, Tunnel and multiphoton ionization of atoms and ions in a strong laser field (Keldysh theory), *Usp. Fiz. Nauk* **174**, 921 (2004) [*Sov. Phys. Uspekhi* **47**, 855 (2004)].
- [41] M. Klaiber, J. Daněk, E. Yakaboylu, K. Z. Hatsagortsyan, and C. H. Keitel, Strong-field ionization via a high-order Coulomb-corrected strong-field approximation, *Phys. Rev. A* **95**, 023403 (2017).
- [42] R. Boge, C. Cirelli, A. S. Landsman, S. Heuser, A. Ludwig, J. Maurer, M. Weger, L. Gallmann, and U. Keller, Probing Nonadiabatic Effects in Strong-Field Tunnel Ionization, *Phys. Rev. Lett.* **111**, 103003 (2013).